Properties of 3Y-TZP zirconia ceramics with graphene addition obtained by spark plasma sintering

Nina Obradović[1,*], Frank Kern[2]

[1]Institute of Technical Sciences of SASA, Knez Mihailova 35/IV, 11000 Belgrade, Serbia

[2]Universität Stuttgart, Institut für Fertigungstechnologie keramischer Bauteile (IFKB), D- 70567 Stuttgart, Germany

ABSTRACT

In this study the influence of graphene addition on the microstructure, phase composition, mechanical, and electrical properties of 3Y-TZP ceramics was investigated. Blends of pure 3Y-TZP and with addition of 1–4 vol. % graphene were prepared by mixing and milling, and they were consolidated by spark plasma sintering (SPS).

Addition of 3 vol. % graphene is necessary to overcome the percolation threshold and obtain electrically conductive composites. However, rising the graphene contents obstructs sinterability. Hence, flexural strength, Young's modulus, and hardness decrease with increasing the graphene content, and the fracture resistance reaches an intermediate maximum at 2 vol. % graphene. Graphene lamellae are oriented orthogonally to the pressing direction. They evidently provide some energy dissipation by crack deflection. TZP-graphene interfaces are very weak. Thus, crack bridging can be neglected.

Keywords: Zirconia, Graphene, XRD, SEM, Mechanical properties, SPS

1. Introduction

Yttrium stabilized zirconia ceramics with high strength and toughness are today applied in machine elements and in biomedical applications such as dental implants, crowns, and bridges [1]. The basis of the excellent mechanical properties is the transformation toughening – a stress induced phase transformation from metastable tetragonal to the stable monoclinic phase. As this transformation is associated with volume expansion and shear, it puts a proceeding crack under compression and slows or stops its growth [2].

*Corresponding author: Dr. Nina Obradović (nina.obradovic@itn.sanu.ac.rs)

Among other isovalent or aliovalent stabilizers added to retain the tetragonal phase at the room temperature, yttrium is the most important today. Trivalent Y^{3+} incorporated as a solid solution into the lattice of zirconia introduces one oxygen vacancy per $2Y^{3+}$ cations for charge neutrality [1]. Besides these stabilizer derived vacancies, vacancies can be introduced by changing sintering conditions. Vacancies in general contribute to stabilizing the high temperature phases (tetragonal and cubic) [3]. 3Y-TZP has also been used as a matrix material for various composite ceramics. TZP-alumina composites (alumina toughened zirconia, ATZ) show enhanced strength and hardness compared to plain Y-TZP [4, 5]. Incorporation of electrically conductive non-oxides such as transition metal carbides, borides, and nitrides (e.g., TiN, WC, TiB_2) in fractions above the percolation threshold makes TZP composite ceramics electrically conductive and electric discharge machinable [6–10]. 3Y-TZP-(30–40 vol. %)TiN and 3Y-TZP-(30–40 vol. %)NbC are commercially applied in manufacturing of customized complex-shape ceramic components.

Recently, carbon materials, such as nano-carbon nanotubes or graphene platelets, have attracted considerable scientific interest to make materials electrically conductive. Nanotubes or platelets, due to their high aspect ratio, can be expected to lead to conductive materials at volume contents lower than for isometric particles [11]. The concept was successfully applied to polymer matrix composites [12]. Recently, the addition of carbon nanostructures in ceramics has become an interesting research topic. A single layered graphene possesses outstanding electrical, thermal, and mechanical properties. Due to a high electron mobility at room temperature ($2.5 \times 105\ cm^2V^{-1}s^{-1}$), exceptional thermal conductivity ($5000\ Wm^{-1}K^{-1}$), and superior mechanical properties with a Young's modulus of 1 TPa, its presence may greatly enhance the electrical conductivity of composites when added to an insulating ceramic matrix [13]. In materials with brittle matrix, such as silicon carbide and alumina, some results indicate the presence of toughening effects [14, 15]. Most toughness values documented – probably due to the small size of samples made by SPS – are, however, obtained by direct crack length measurements, which may lead to misleading values [16]. Others use SEPB tests with blunt notches, which are also not suitable to determine the fracture resistance of ultrafine grain materials [17, 18]. Furthermore, it is known that attention must be paid to the source of graphene used and processing technology, in order to obtain a homogeneous dispersion of graphene in the parent matrix. A good overview of existing technologies is given by Markandan [19]. Graphene may be introduced by

mechanical alloying, colloidal mixing, or by more sophisticated chemical routes such as polymer derived ceramics or sol-gel. Publications on Y-TZP-graphene are not very frequent and most of them cover a graphene or graphene oxide content range which is far too low for ED-machining target applications [17].

Graphene may influence the tetragonal to monoclinic and cubic phase ratios in the matrix, which could affect the fracture toughness. Moreover, the high ratio of graphene compared to matrix grains may induce texture effects occurring during shaping/sintering, which have to be considered. Therefore, the understanding of interfacial structures and properties is crucial in order to obtain high performance ceramic/graphene composites.

The crucial questions for the development of ED-machinable TZP-graphene composites are: how much graphene has to be added to obtain the required electrical conductivity and what is the effect on mechanical properties and possible applications. The basic conductivity threshold is at 1 S/m (in commercially available performing ED-machinable ceramics several orders of magnitude higher is required) [6, 20]. In this study, a commercially available high strength alumina doped 3Y-TZP material with a proven track record in dental applications was blended without and with the addition of 1–4 vol. % of graphene, consolidated by spark plasma sintering (SPS), and subsequently tested, in order to obtain electrical conductive ceramic and to investigate the influence of graphene addition on sinterability and mechanical properties of zirconia-based ceramics.

2. Experimental procedure

For this study a standard 3Y-TZP zirconia powder (TZ 3Y-SE, S_{BET} = 7 m²/g Tosoh, Japan) was used as matrix material. Graphene nanoplatelet aggregates (S_{BET} = 7 m²/g, ABCR, Germany) were added in fractions in the range 1–4 vol. % in 1 vol. % increments. (Assuming a bulk density of ~ 2.2 g/cm³ for graphene and ~ 6.1 g/cm³ for 3Y-TZP, this corresponds to volume contents of 0–10.2 vol. % provided the full density is achieved.)

The individual batches of 100 g powder mixture were attrition milled for 4 h at 400 rpm in 250 ml 2-propanol, with 3Y-TZP milling balls of 2 mm diameter. The grinding media were then separated and the resulting slurry was dried at 45 °C overnight. The dry residue was screened through a 100 µm mesh to provide the press ready feedstock.

Discs of 45 mm diameter were spark plasma sintered (FCT Anlagenbau, Germany) at a final temperature of 1350 °C at 60 MPa axial pressure and 5 min dwell in graphite paper clad graphite dies. An initial load of 2 MPa was applied at the start of the SPS, it was elevated to 60 MPa after the sintering temperature of 1100 °C was reached, and kept during further heating to the final temperature and dwell. Sintering was carried out in a vacuum using a heating rate of 20 K/min. Two discs of approx. 30 g of each composition were SPS sintered.

Samples were lapped with 15 µm diamond suspension and afterwards polished using 15 µm, 3 µm, and 1 µm diamond suspensions until a mirror-like surface was achieved (Struers Rotopol, Denmark). Young's modulus and Poisson's ratio were measured on entire discs by using the acoustic method (IMCE, Belgium). Densities were determined according to the Archimedes principle (Kern ABS, Germany) in distilled water. Furthermore, Vickers hardness HV10 and indentation fracture resistance by direct crack length measurement (DCM) were carried out on polished discs. DCM (five HV10 indents each) tests were evaluated according to the models of Evans, Anstis, and Niihara [21–23]. For the bending strength tests and fracture resistance determination by indentation strength in bending (ISB), the two thinner discs were cut into bars of 4 mm width using a diamond wheel (Struers Accutom 50, Denmark). Sides of the bars were lapped using 15 µm diamond suspension and edges were beveled using a 20 µm diamond disc to avoid any influence of cutting defects on the measurements. Bending strength (10 specimens each) was determined in a 4-pt setup with 20/10 mm outer/inner span. Crosshead speed was set to 0.5 mm/min (Z100, Zwick Ulm, Germany). ISB tests were performed with the same setup using a crosshead speed of 2.5 mm/min to avoid subcritical crack growth. Notching was carried by placing a HV10 indent in the middle axis of the tensile side of the bars with cracks parallel and perpendicular to the sides. The residual strength was measured immediately after notching and $K_{IC,ISB}$ calculated according to the model of Chantikul [24].

Electrical conductivities of the materials were determined by using the 4 point measurement method and using polished bending bars of minimum 40 mm length, 3.9 mm width and ~ 2 mm thickness. The microstructure of polished and thermally etched samples (Hydrogen at 1300 °C for 5 min), as well as the fracture surface, were studied by SEM (Zeiss Gemini, Germany, secondary electrons, 10 kV, in lens technology). The phase composition of the samples was investigated by XRD (Bruker D8, Germany, CuKα, Bragg Brentano setup, 2-theta 27–33 °, and integration of (111)-*m*, (111)-*m*, and (101)-*t* reflections).

A basic ED-machining test was carried out by die sinking with copper electrodes in an oil-based dielectric fluid (AEG Elotherm, Germany).

3. Results and discussion

3.1. Mechanical and electrical properties

All samples showed relative theoretical densities (TD) higher than 97.5 % (based on the rule of mixture, assuming the tetragonal phase for zirconia, and $\rho_{TD(3Y\text{-}TZP)} = 6.08\ gcm^{-3}$, $\rho_{TD(graphene)} = 2.23\ gcm^{-3}$). Samples with up to 1 vol. % graphene showed densities higher than 99.2 % TD.

Figure 1. Young's modulus and relative density of sintered samples.

A further increase of the graphene contents seems to impede the densification. In line with the density data, the Young's modulus decreases almost linearly from 212.9 GPa for 3Y-ZTA to 159.7 GPa for 3Y-ZTA-4G (see Figure 1), and follows the trend of the density behavior. An increase of Young's modulus, as may be expected from the rule of mixture considering that the high in-plane stiffness of graphene, was not observed.

Figure 2 shows the hardness and bending strength of the TZP-graphene composites. Both values decline with increasing the graphene content, whereas the hardness shows a linear decline and the strength shows an exponential decline. Both curves reflect the trend to lower the density and increase the porosity and, thereby, the amount of structural defects.

Figure 2. Vickers hardness HV10 and 4pt bending strength of sintered samples.

Figure 3 shows the fracture resistance determined by the DCM method using the Palmquist crack model by Niihara [23] and by the ISB method. The ISB test leads to a trend with an intermediate toughness maximum at 1–2 vol. % graphene and a progressive decline at elevated graphene contents. The DCM test shows no clear trend. The ISB test seems more reliable as it involves no subjective errors in measuring the crack length. Still, the different

values may hint at a different ratio between the intrinsic toughness and the R-curve behavior in both materials.

Figure 3. Fracture resistance values K_{DCM} and K_{ISB} of sintered samples.

The DCM toughness values according to Evans and Anstis are not shown. They show identical trends, either on a reduced level (Anstis) or on an almost identical level (Evans).

The electrical conductivity of the investigated materials showed values of 58.31 S/m for 3Y-ZTA-3G and 291.55 S/m for 3Y-ZTA-4G. This strong increase in conductivity with the fraction of the added graphene reflects the behavior at the edge of the percolation threshold. The conductivity of materials with lower graphene content was not measurable.

3.2. Microstructure

SEM micrographs obtained on polished and thermally etched sintered samples are presented in Figure 4. A homogenous fully dense microstructure with no porosity is present within the reference sample 3Y-TZP. Grains have a size of < 500 nm. Small graphene platelets in the sample with 1 vol. % graphene are isolated and homogenously distributed in the matrix. The shape, size, and size distribution of graphene change with increasing the graphene fraction. In samples with 2 vol. % graphene, much longer graphene lamellae of up to 1 µm length appear besides smaller fragments. This trend is amplified in samples with 3 vol. %. Here an increasing number of multilayer inclusions can be observed. In samples with 4 vol. %, the preferred orientation of platelets orthogonal to the pressing direction breaks down some larger curled. Folded graphene structures are observed, which strongly obstruct the structure. With increasing the volume fraction of graphene, a decrease in density of the material and the occurrence of pores is observed. Pores are only present in the vicinity of graphene platelets. This observation is in line with measured densities and Young's moduli.

Figure 4. SEM micrographs of sintered samples obtained on thermally etched surface: a) 3Y-ZTA, b) 3Y-ZTA-1G, c) 3Y-ZTA-2G, d) 3Y-ZTA-3G, and e) 3Y-ZTA-4G.

Figure 5. SEM micrographs of sintered samples obtained on fractured surface: a) 3Y-ZTA, b) 3Y-ZTA-1G, c) 3Y-ZTA-2G, d) 3Y-ZTA-3G, and e) 3Y-ZTA-4G.

Figure 5 presents SEM micrographs obtained on fractured surfaces of all sintered samples. The plain 3Y-ZTA sample shows a mixed fracture behavior with predominant intergranular fracture. With graphene addition, the fracture mode is slightly shifted exhibiting some more transgranular fractures. In samples with only 1 vol. % graphene, a very homogeneous distribution of graphene in the TZP matrix is observed, platelets are well embedded, and the porosity in the vicinity of the graphene structures is not detected. The fracture surfaces of samples with 2–3 vol. % graphene look very similar: larger platelets form typical pullout structures, fragments either stick in one of the fracture faces or leave slot-shaped voids in the counterpart. Areas previously covered with graphene are very smooth, indicating very poor interfacial strength. The graphene platelets as such seem to have a very high strength as they are never fractured. This is in line with expectations. The fracture surfaces in these composites are much rougher than in case of plain 3Y-TZP, which indicates the presence of toughening effects by crack deflection.

3.3. Phase composition

Figure 6. XRD patterns of all sintered samples obtained on polished surface.

The XRD patterns obtained on the surface as well as on the fracture phase in the range 27–33 ^{o} 2θ, reveal only the presence of the tetragonal (*101*) reflection at 30.18 ^{o} in all the sintered composites (see Figure 6). There is no observation of appearance of the monoclinic phase in ZrO_2 with the addition of graphene, indicating that in this observed region the addition of graphene does not induce $t \rightarrow m$ ZrO_2 phase transformation. Fracture surfaces (not shown) were checked. The monoclinic phase was not found. This shows that there is no measurable contribution to toughness by the transformation toughening. The presence of the cubic ZrO_2 phase was not observed. In the range 70–75 ° 2θ only the tetragonal (*004*) and (*400*) peaks were detected.

3.4. ED-machinability

Samples containing 3 and 4 vol. % graphene were checked for ED machinability on a die sinking machine. The basic test showed that the materials can be electrically contacted. Some sparks were observed, but a controlled material removal process, which would be necessary for technical exploitation, was not possible.

4. Discussion

In this work a mixing and milling approach was tested to manufacture Y-TZP/graphene composites. It can be stated that the chosen milling procedure (4 h attrition milling in 2-propanol) efficiently deagglomerates the Y-TZP. The ability of this procedure to break up the graphene aggregates of the graphene fraction is low. At 1 vol. % graphene, only small fragments are produced, which are well embedded into the TZP matrix, and do not cause any severe defects of pores. At an increasing fraction of graphene, the milling efficiency is visibly reduced. Larger fragments of multilamellar graphene platelets are left besides smaller fragments. It may be speculated that when higher fractions of graphene are added, some lubrication effects appear that reduce the milling efficiency.

These large fragments align orthogonally to the direction of loading and lead to a strong anisotropy. Moreover, it can be seen that the stress transfer between the matrix and graphene reinforcement is not very efficient. Cracks are easily deflected along TZP graphene interfaces, which should *a priori* lead to improved toughness. Very smooth interfaces and the ease of pullout indicate that the interlocking between the matrix and reinforcement is very weak. This observations were also found in the literature, but interpreted in a different manner [17, 25, 26]. At very high graphene contents, curled multlayer inclusions are formed. Larger fractions of graphene introduce pores and microstructural defects, which lead to deteriorated strength, hardness, and Young's modulus. Fracture resistance values determined by ISB test using sharp notches and measuring residual strength show only an incremental increase in toughness up to 2 vol. % graphene, and a subsequent embrittlement. DCM test show much higher non-systematical fluctuations and give rise to the suggestion that enhanced toughness values reported in earlier studies could be artifacts of the measuring technology (too low load [27]), and anisotropic microstructure [17, 26].

Another fact supporting the statement of weak grain boundaries is the phase composition. Graphene has a negative in-plane CTE, whereas CTE of TZP is positive. It was expected that during cooling strong residual stress should evolve between graphene and TZP, leaving TZP under tension and graphene under compression. This effect may cause phase transformation of zirconia during cooling or during fracture due to the superposition of the residual and applied stress. However, a phase transformation was not observed, neither in bulk material, nor in the fractured specimen. This fact further supports the statement that the interface is weak. Most probably the graphene platelets under compression are just clamped between very smooth zirconia surfaces and slide relative to the surrounding TZP. Thereby, a relaxation of the stress occurs and possibly also a microscopic in situ delamination during cooling. As this effect should scale with size of graphene inclusions, it was not observed in the material containing 1 vol. % graphene. The results are in line with results of Chen who succeeded in introducing very small graphene platelets [26]. In multilayer structures, such as at higher graphene contents, this is even more facile. Sintering conditions were chosen correctly. The TZP made from coprecipitated mixture is super-saturated with yttrium, at the sintering temperature of 1350 °C tetragonal and cubic phase coexist in a ratio of ~ 85/15 [28]. There was, however, no cubic phase detected. Supersaturation of the stabilizer prevails and the phase segregation is not observed [29]. As the graphene containing materials also show no indications of the cubic phase, the presence of carbon did not lead to incorporation of carbon into the anionic lattice of zirconia. The formation of reduction-induced vacancies further contributes to stabilization. The negative side-effect is, however, a very moderate toughness of the material as transformation toughening effects are completely absent. This, however, allowed the establishment of the – apparently not existing – toughening effect of graphene without superposition of transformation toughening effects. As expected, the graphene addition leads to a certain electrical conductivity in the composites, which is higher that the required minimum threshold for ED-machinability [20]. Compared to commercially ED-machinable ceramics made conductive by the addition of transition metal carbides or nitrides, the measured conductivity is lower by a factor of 100-1000, which may be (together with the anisotropy of the materials) the cause for the failure of the ED-machining test [30]. However, the obtained conductive ceramic materials can be used in technical applications where removal of electrostatic buildup is required, in devices where an electric contact is

required for sensing and measurements, and as absorbing materials for radiofrequency and microwave applications.

Graphene has two basic roles. The first one is to improve the electrical conductivity. In that sense, small, randomly oriented fragments are more efficient. The second role is to boost the strength and toughness. For this role, larger single lamella able to bridge cracks and bear high stress would be favored. The axial pressing technology, however, always leads to laminate structures with a strong anisotropy and low coherence between the matrix and dispersion.

5. Conclusion

Composites 3Y-TZP-graphene were made electrically conductive by addition of graphene in fractions $\geq$ 3 vol. %. The addition of graphene leads to a progressive decline in hardness, strength, and Young's modulus. Any significant increase of toughness was not observed.

The analysis of the fracture surface shows indications of strong pullout effects. It also shows that the bonding of the matrix and reinforcement is relatively weak as contact areas are perfectly smooth. Crack deflection is facilitated, but stress transfer to the reinforcement is not strong enough.

Results indicate that mixing and milling approach seems to give convenient microstructures for composites with 1 vol. % – 2 vol. % graphene. Higher graphene fractions ($\geq$ 3 vol. %) result in a broad graphene size distribution and the appearance of multilayer lamellae. Consolidation by spark plasma sintering leads to highly anisotropic materials. Further studies will be necessary to achieve the target of producing technically relevant ED-machinable composites. However, the obtained conductive ceramic materials can find various applications in electrical engineering, e.g., for draining static electricity, providing contacts for sensing and measurements, and as absorbing materials for radiofrequency and microwave applications.

Acknowledgement

This study was conducted within the DAAD scholarship project titled "*Development of materials and manufacturing technologies for electric discharge machinable Zirconia–CNT/Graphene composites*".

6. References

[1] Hannink, R. H. J., Kelly, P., Muddle, B. C.: "Transformation Toughening in Zirconia-Containing Ceramics", J. Am. Ceram. Soc., 83 [3] (2000) 461–87.

[2] Kelly, P. M., Rose, L. R. F.: "The martensitic transformation of ceramics – its role in transformation toughening", Progr. Mat. Sci., 67 (2002) 463–557.

[3] Hillert, M: Thermodynamic Model of the Cubic - Tetragonal Transition in Nonstoichiometric Zirconia, J. Am. Ceram. Soc., 74 [8] (1991) 2005–2006.

[4] Tsukuma, K., Ueda, K, Shimada K.: "Strength and Fracture Toughness of Isostatically Hot-Pressed Composites of Al_2O_3 and Y_2O_3-Partially-Stabilized ZrO_2", J. Am. Ceram. Soc., 68 [1] (1985) C4–C5.

[5] Kern, F., Gadow, R.: „Alumina toughened zirconia from yttria coated powders", J. Eur. Ceram. Soc., 32 (2012) 3911–8.

[6] U. Schmitt-Radloff, F. Kern, R. Gadow, Wire-electrical discharge machinable alumina zirconia niobium carbide composites – Influence of NbC content, J. Eur. Ceram. Soc. 37 (2017) 4861–4867.

[7] P. Ninz, R. Landfried, F. Kern, R. Gadow, Electrical discharge machining of metal doped Y-TZP/TiC nanocomposites, J. Eur. Ceram. Soc. 35 (2015) 4031–4037.

[8] K. Vanmeensel, S. G. Huang, A. Laptev, S. A. Salehi, A. K. Swarnakar, O. Van der Biest, J. Vleugels, Pulsed electric current sintering of electrically conductive ceramics, J. Mater. Sci. 43 (2008) 6435–6440.

[9] S. G. Huang, K. Vanmeensel, O. Van der Biest, J. Vleugels, Development of ZrO_2-WC composites by pulsed electric current sintering, J. Eur. Ceram. Soc. 27 (2007) 3269–3275.

[10] B. Lauwers, J. P. Kruth, W. Liu, W. Eeraerts, B. Schacht, P. Bleys, Investigation of material removal mechanisms in EDM of composite ceramic materials, J. Mater. Process. Technol. 149 (2004) 347–352.

[11] I. Balberg, D. Azulay, D. Troker, O. Millo, Percolation and tunneling in composite materials, Int. J. Mod. Phys. B 18 (2004) 2091–2121.

[12] Tang, C., Long. G., Hu, X., Wong, K.W., Lau, W.M., Fan, M., Mei, J., Xu, T., Wang, B., Hui, D: Conductive polymer nanocomposites with hierarchical multi-scale structures via self-assembly of carbon-nanotubes on graphene on polymer-microspheres, Nanoscale 6 [14] (2014) 7877–88.

[13] A. Gallardo-López, I. Márquez-Abril, A. Morales-Rodríguez, A. Muñoz, R. Poyato, Dense graphene nanoplatelet/yttria tetragonal zirconia composites: Processing, hardness and electrical conductivity, Ceram. Inter. 43 (2017) 11743–11752.

[14] M. Belmonte, A. Nistal, P. Boutbien, B. Román-Manso, M. I. Osendi, P. Miranzo: Toughened and strengthened silicon carbide ceramics by adding graphene-based fillers, Scripta Materialia, 113 2016 127–130.

[15] H. Porwal, P. Tatarko, S. Grasso, J. Khaliq, I. Dlouhy, M. J. Reece: Graphene reinforced alumina nano-composites, Carbon, 64 (2013) 359–369.

[16] Quinn, G.D., Bradt, R.C: "On the Vickers Indentation Fracture Toughness Test", J. Am. Ceram. Soc., 90 [3] (2007) 673–680.

[17] S. Li, Z. Xie, Y. Zhang,Y. Zhou: Enhanced toughness of zirconia ceramics with graphene platelets consolidated by spark plasma sintering, Int J Appl Ceram Technol. 14 (2017) 1062–1068.

[18] H. Fischer, A. Waindich, R. Telle: Influence of preparation of ceramic SEVNB specimens on fracture toughness testing results, Dental materials, 24 (2008) 618–622.

[19] K. Markandan, J.K. Chin, M. T. Tan: Recent progress in graphene based ceramic composites: a review, J. Mater. Res., Vol. 32, No. 1, Jan 13, 2017.

[20] Panten, U. Funkenerosive Bearbeitung von elektrisch leitfähigen Keramiken; PhD Thesis, RWTH Aachen, 1990.

[21] A. G. Evans, E. A. Charles, Fracture toughness determinations by indentation, J. Am. Ceram. Soc. 59 (1976) 371–372.

[22] G. R. Anstis, P. Chantikul, B. R. Lawn, D. B. Marshall, A critical evaluation of indentation techniques for measuring fracture toughness: I direct crack measurements, J. Am. Ceram. Soc. 64 (1981) 533–538.

[23] K. Niihara, A fracture mechanics analysis of indentation-induced Palmqvist crack in ceramics, J. Mater. Sci. Lett. 2 (1983) 221–223.

[24] P. Chantikul, G. R. Anstis, B. Lawn, D. Marshall, A critical evaluation of indentation techniques for measuring fracture toughness: II Strength method, J. Am. Ceram. Soc. 64 (1981) 539–543.

[25] J. Liu, H. Yan, M. J. Reece, K. Jiang, Toughening of zirconia/alumina composites by the addition of graphene platelets, J. Eur. Ceram. Soc. 32 (2012) 4185–4193.

[26] F. Chen, D. Jin, K. Tyeb, B. Wang, Y.-H. Han, S. Kim, J. M. Schoenung, Q. Shen, L. Zhang, Field assisted sintering of graphene reinforced zirconia ceramics, Ceram. Inter. 41 (2015) 6113–6116.

[27] R.F. Cook, L.M. Braun, W.R. Cannon: Trapped cracks at indentations Part I Experiments on yttria-tetragonal zirconia polycrystals, J. Mat. Sci. 29 (1994) 2933–42.

[28] Chen, M., Hallstedt, B., Gauckler, L.: "Thermodynamic modeling of the ZrO_2–$YO_{1.5}$ system", Solid State Ionics 170 (2004) 255–274.

[29] Matsui, K., Horikoshi, H., Ohmichi, N., Ohgai, M.,Yoshida, H., Ikuhara, Y: "Cubic-Formation and Grain-Growth Mechanisms in Tetragonal Zirconia Polycrystal", J. Am. Ceram. Soc., 86 [8] (2003) 1401–8.

[30] Gommeringer, A.; Schmitt-Radloff, U.; Ninz, P.; Kern, F.; Klocke, F.; Schneider, S.; Holsten, M.; Klink, A. ED-machinable Ceramics with Oxide Matrix: Influence of Particle Size and Volume Fraction of the Electrical Conductive Phase on the Mechanical and Electrical Properties and the EDM Characteristics. Procedia CIRP 2018, 68, 22–27.

Figure

Click here to download high resolution image

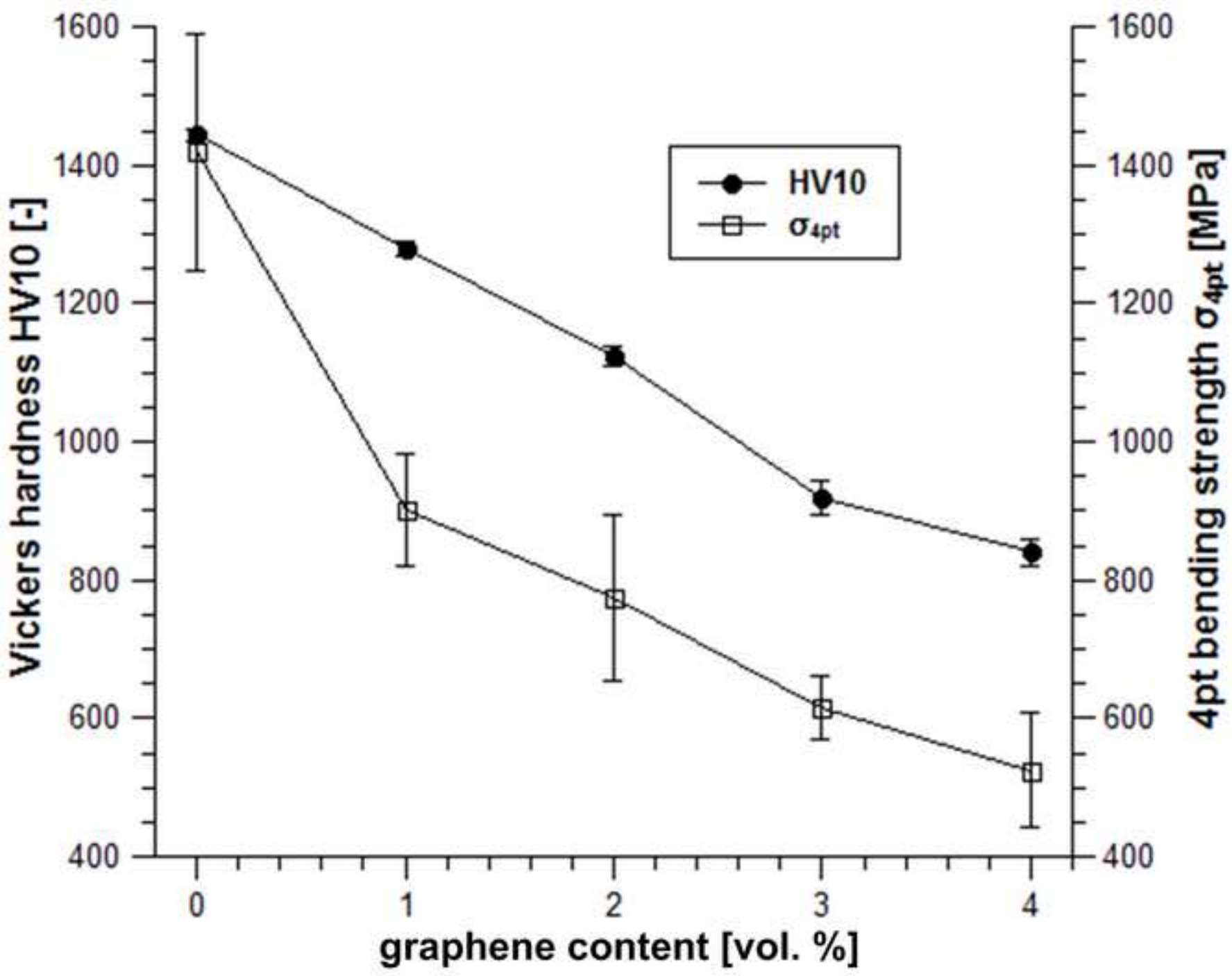

Figure

Click here to download high resolution image

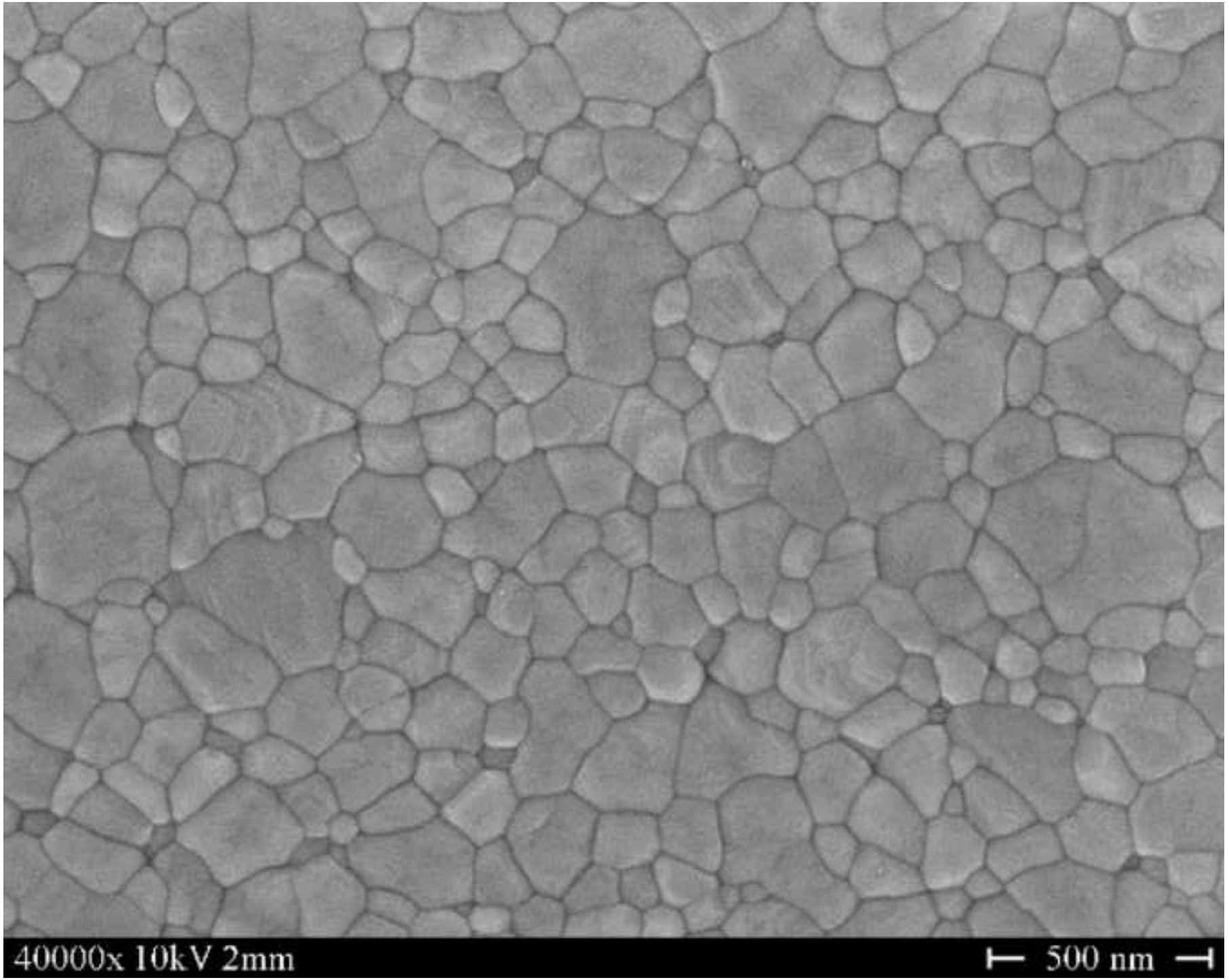

Figure

Click here to download high resolution image

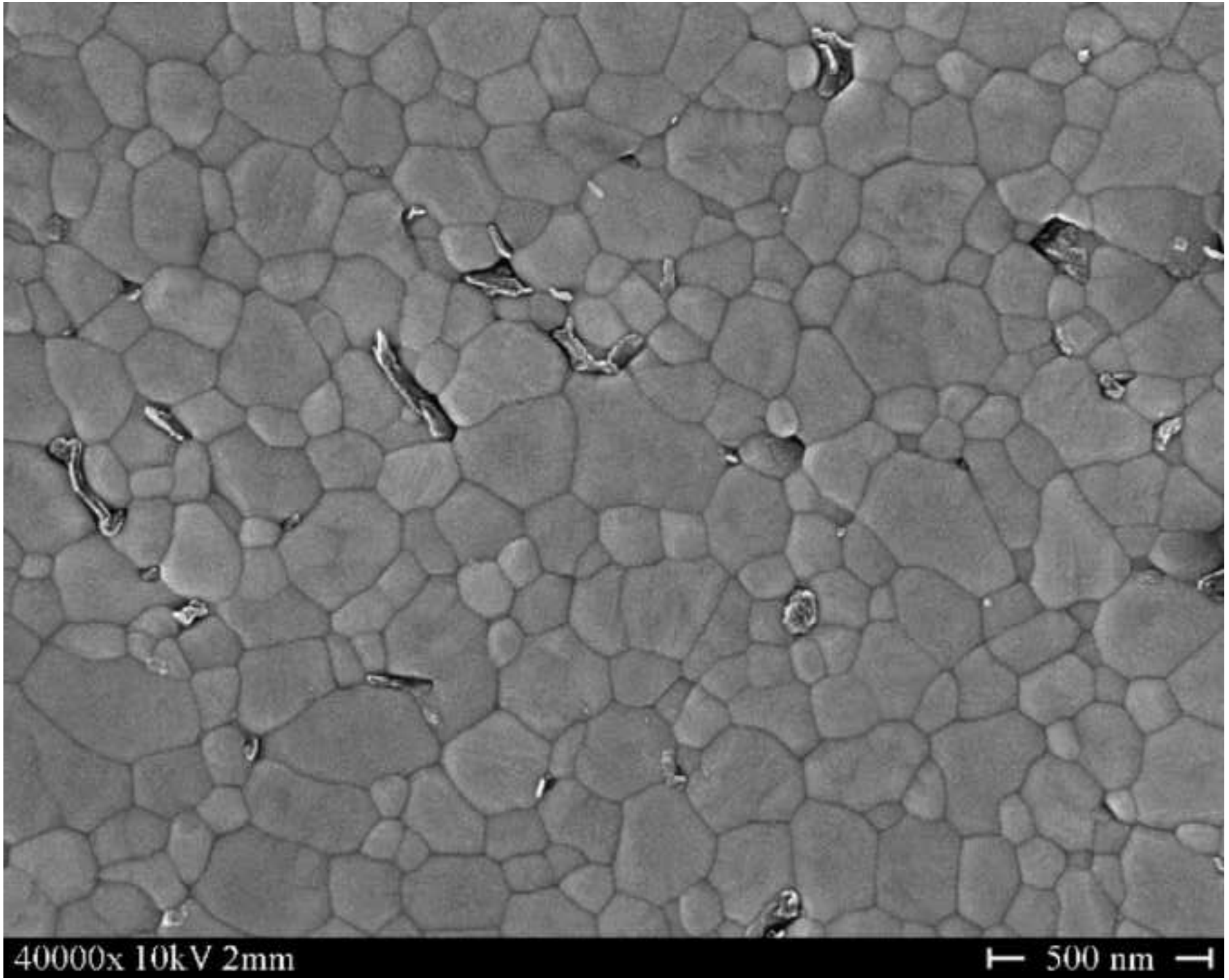

Figure

Click here to download high resolution image

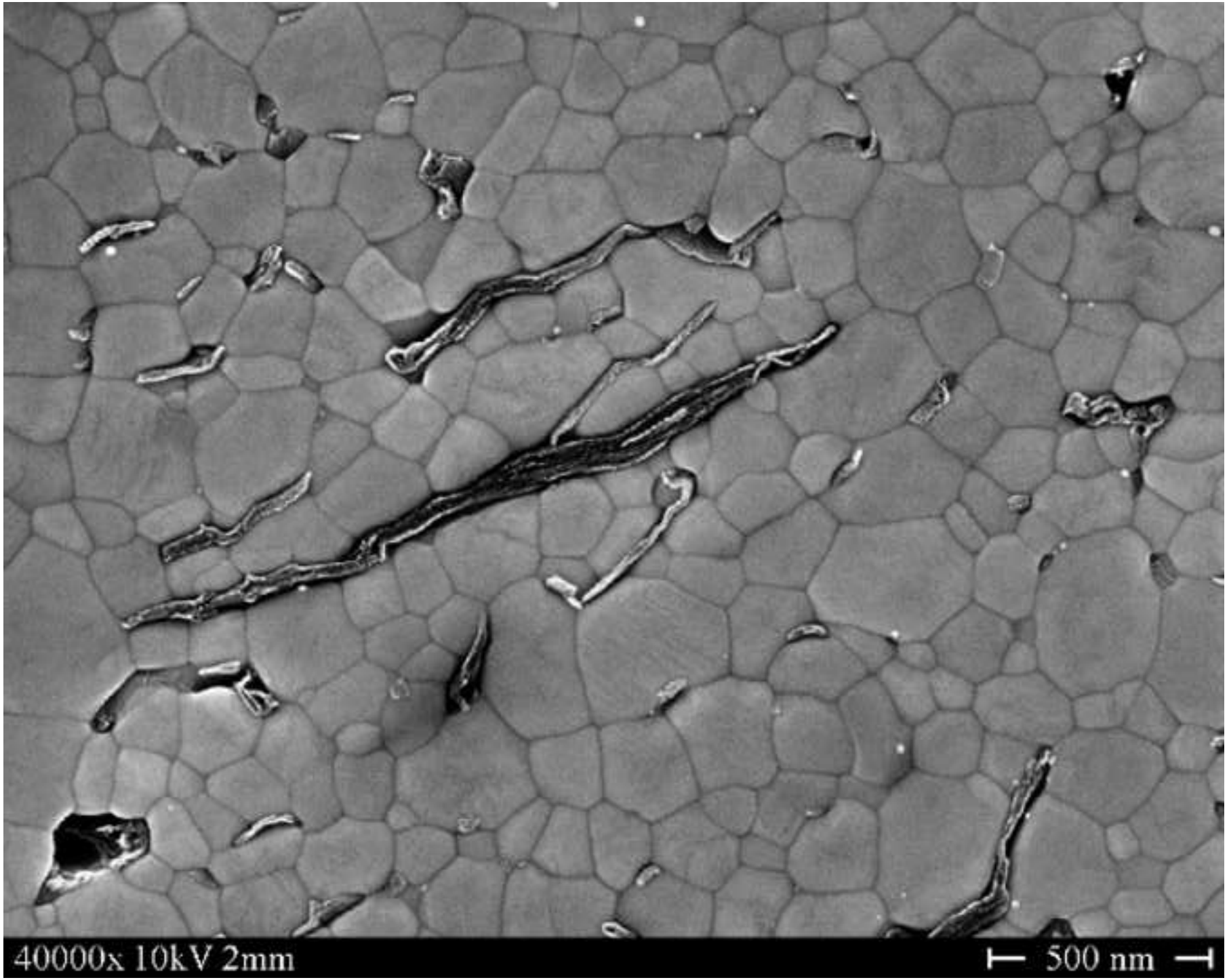

Figure

Click here to download high resolution image

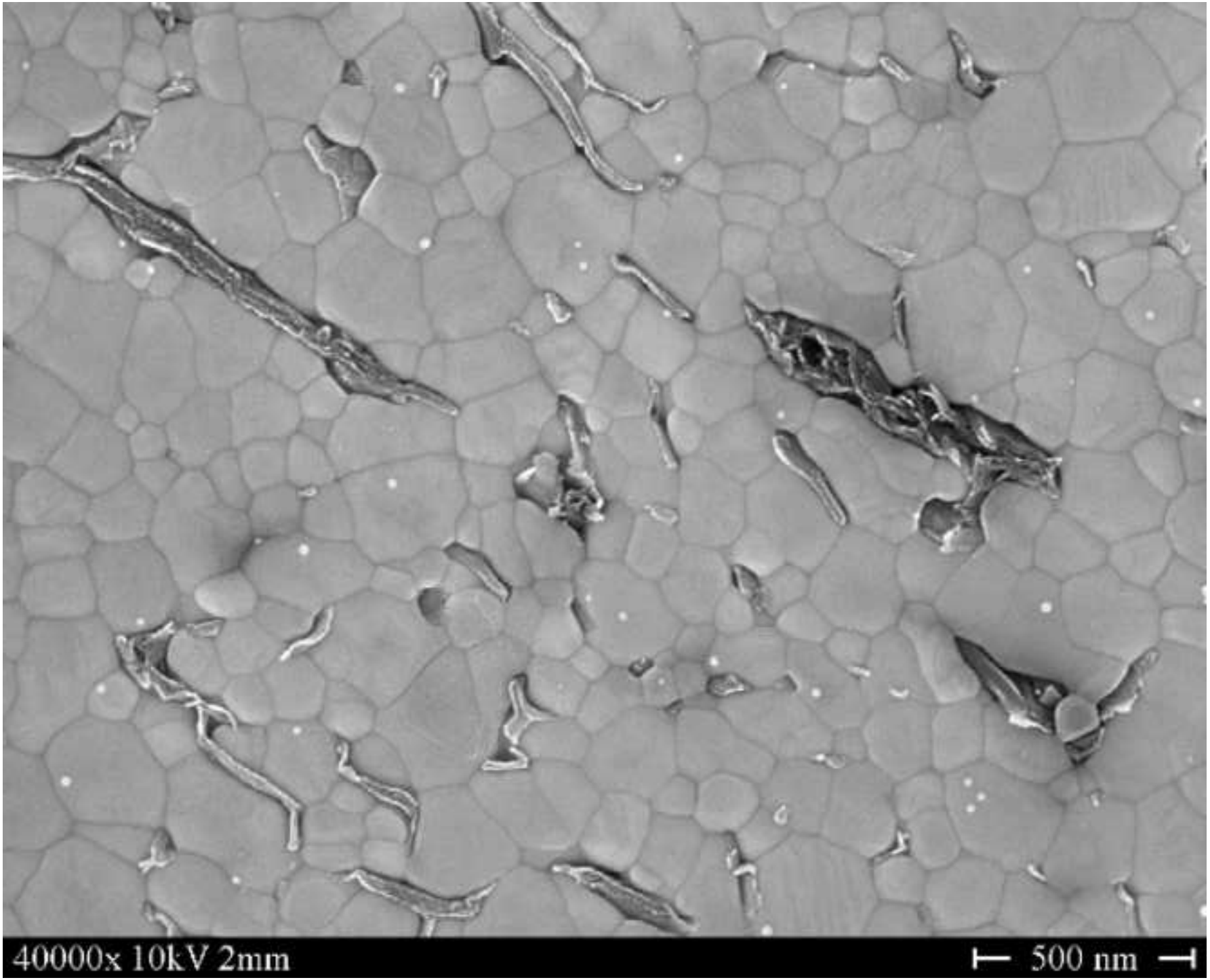

Figure

Click here to download high resolution image

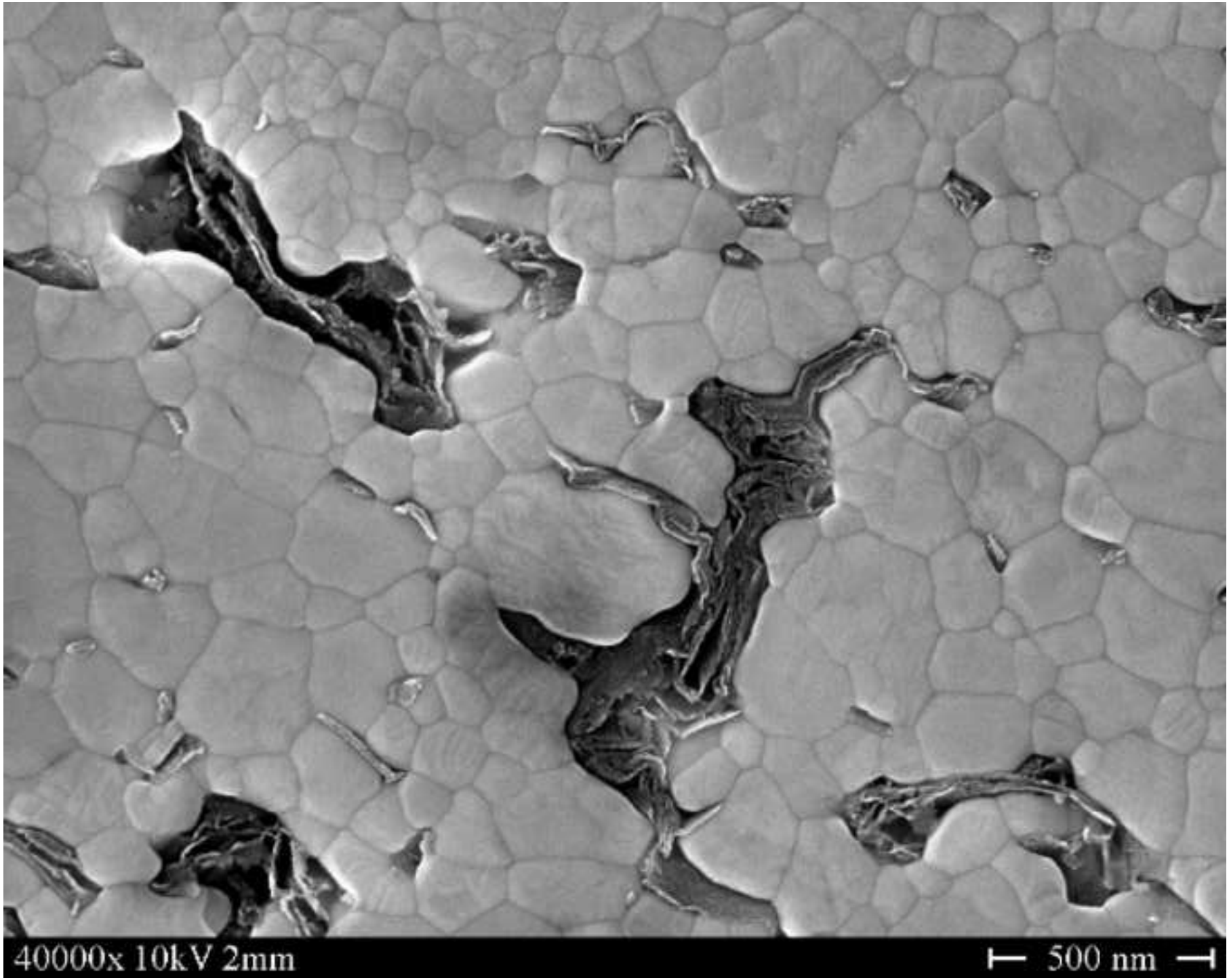

Figure

Click here to download high resolution image

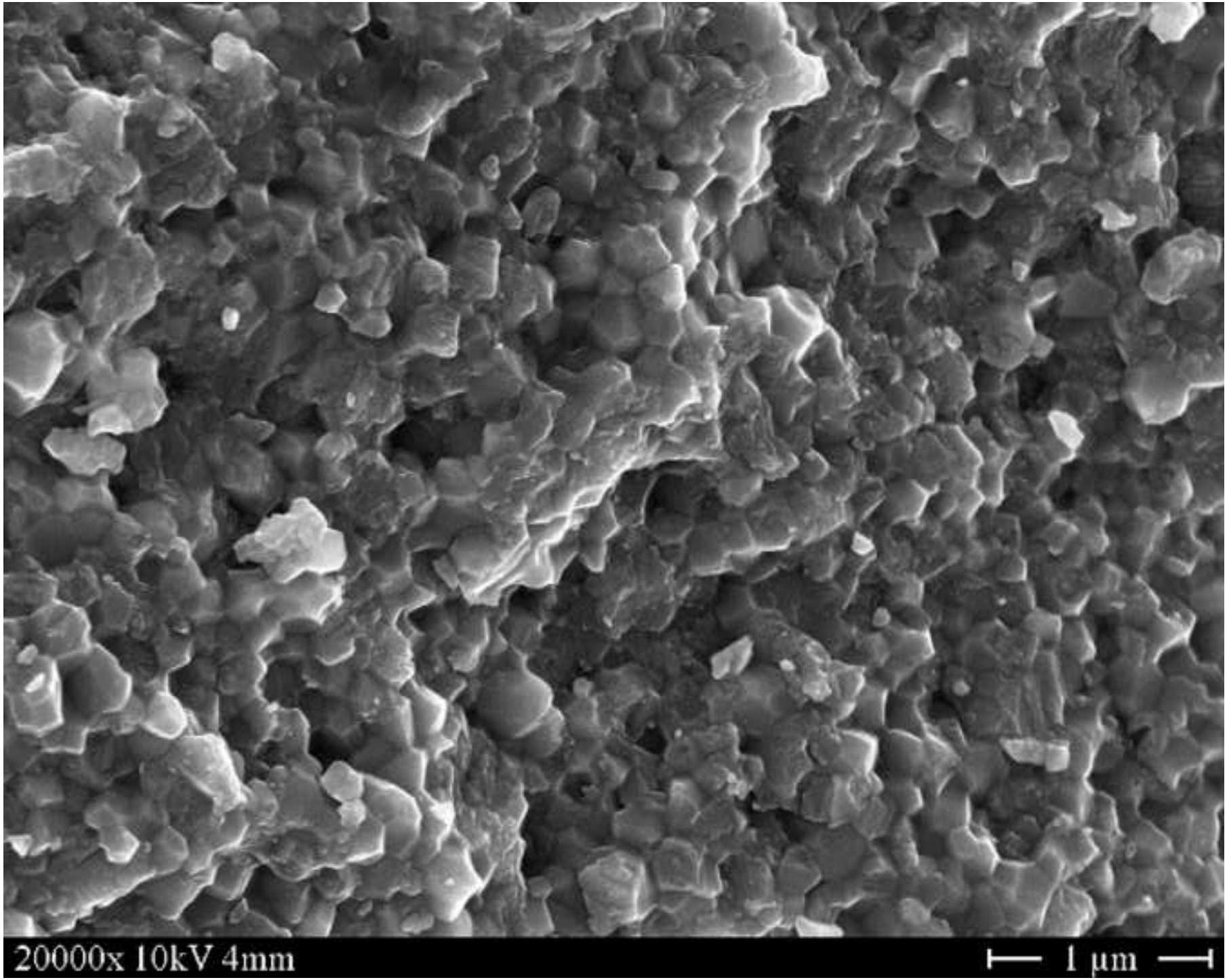

Figure

Click here to download high resolution image

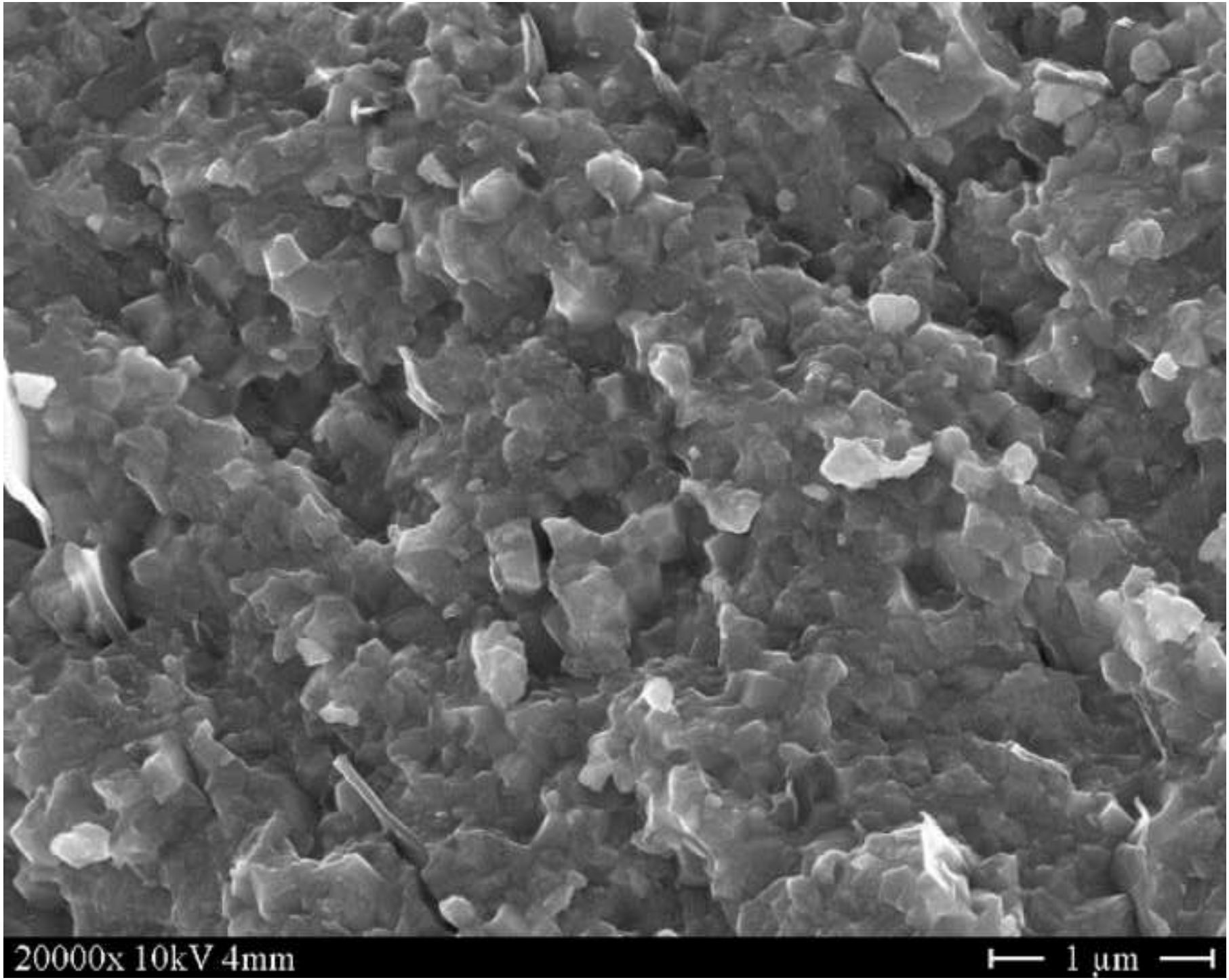

Figure

Click here to download high resolution image

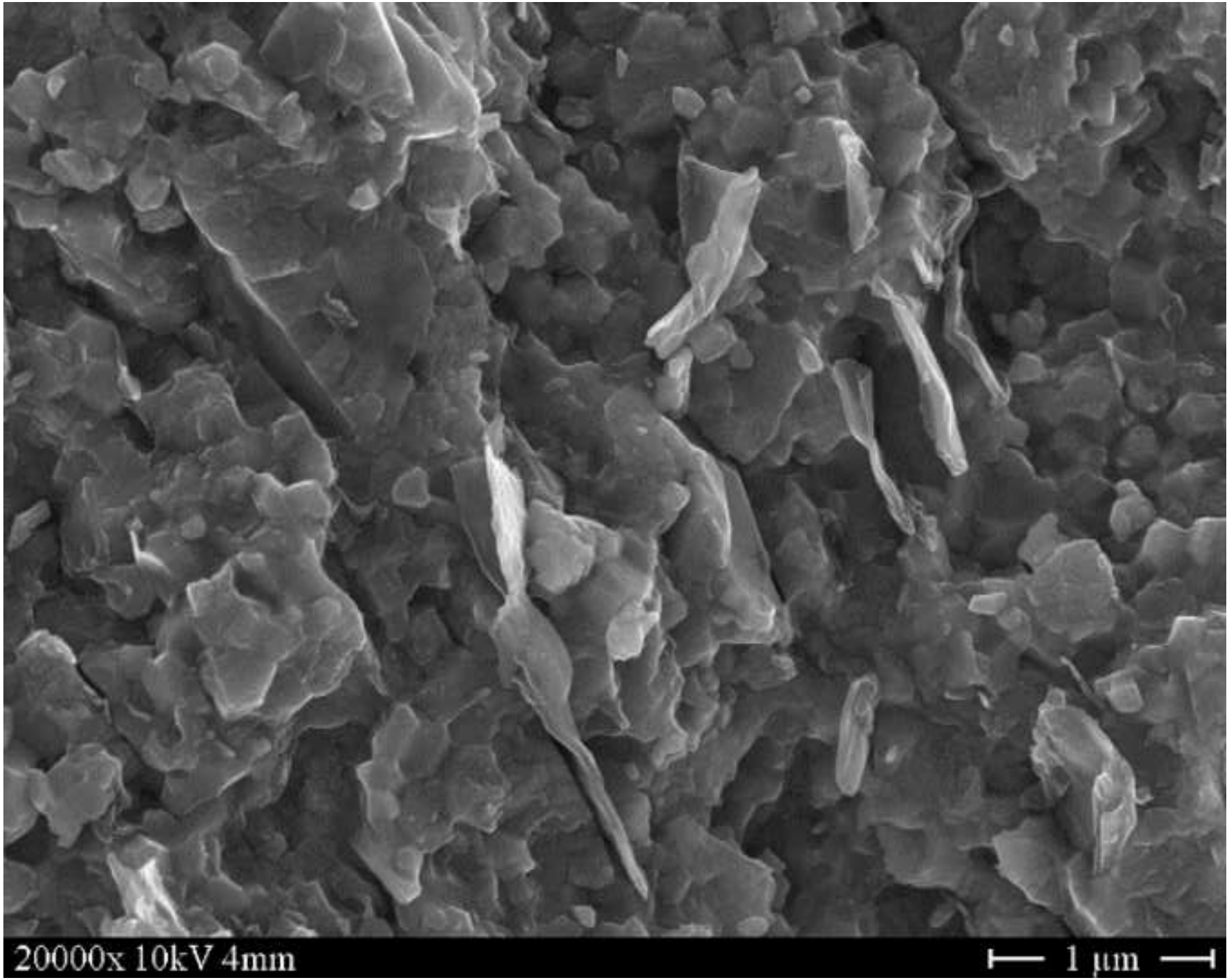

Figure

Click here to download high resolution image

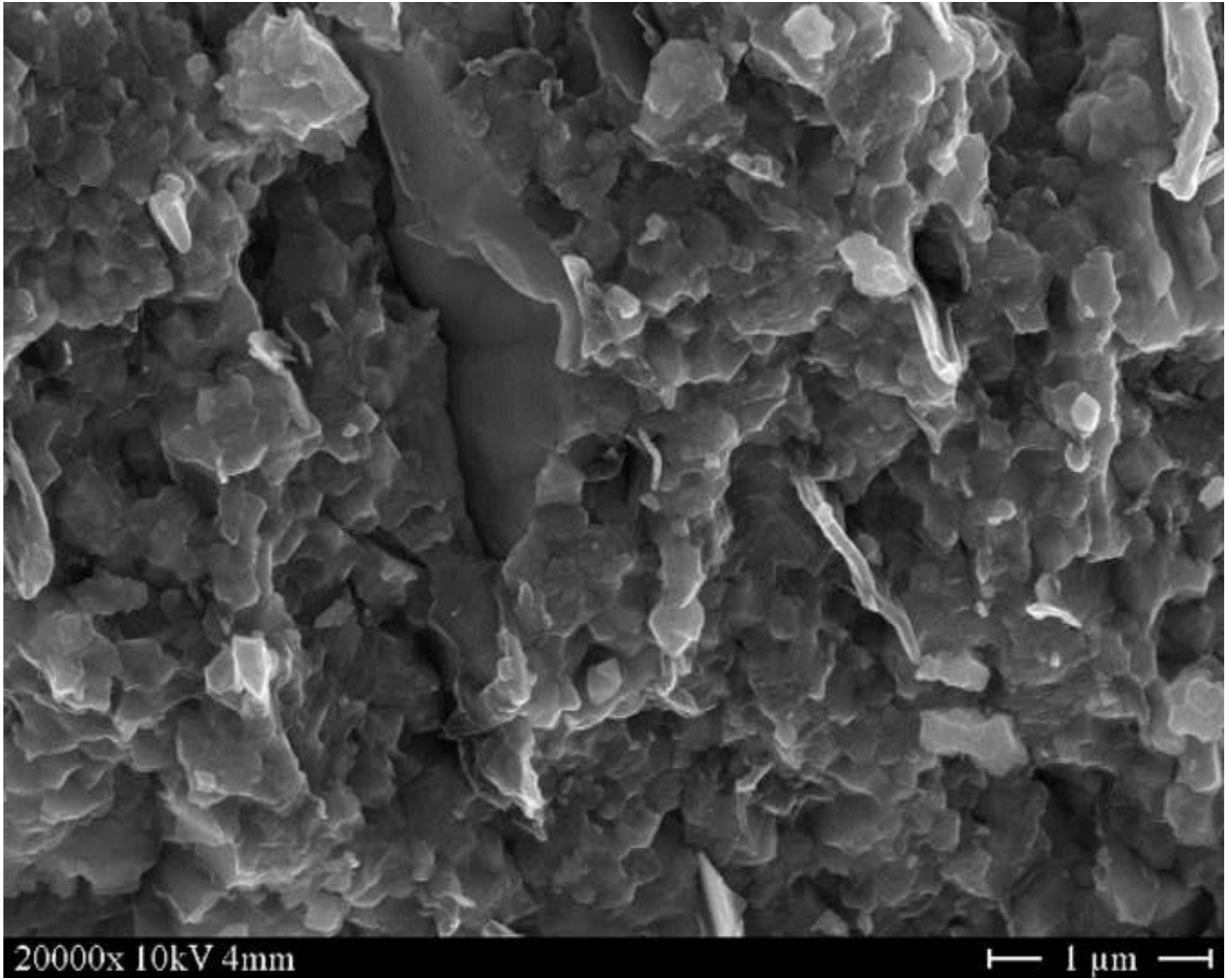

Figure

Click here to download high resolution image

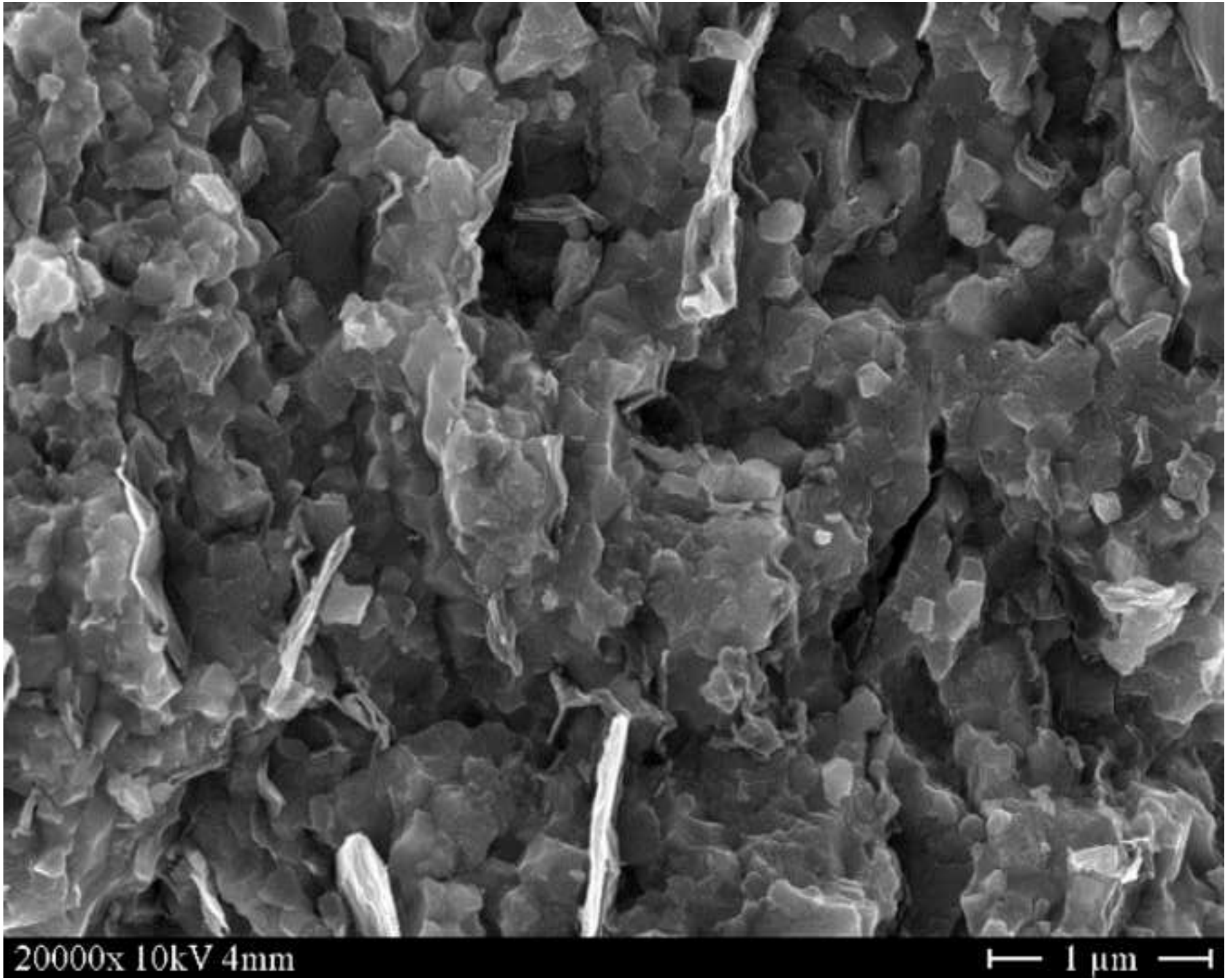

Figure

Click here to download high resolution image

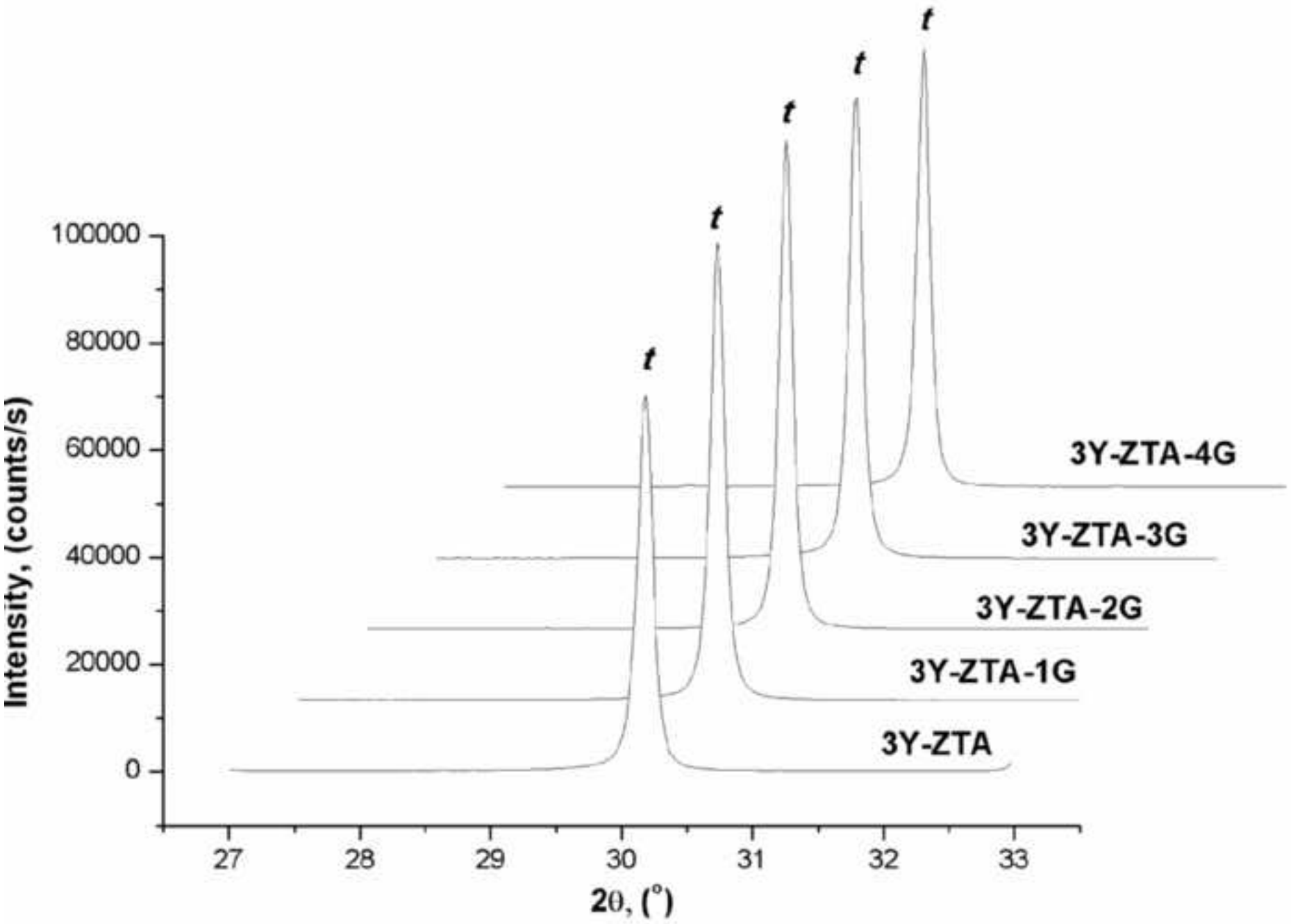

Figure
Click here to download high resolution image

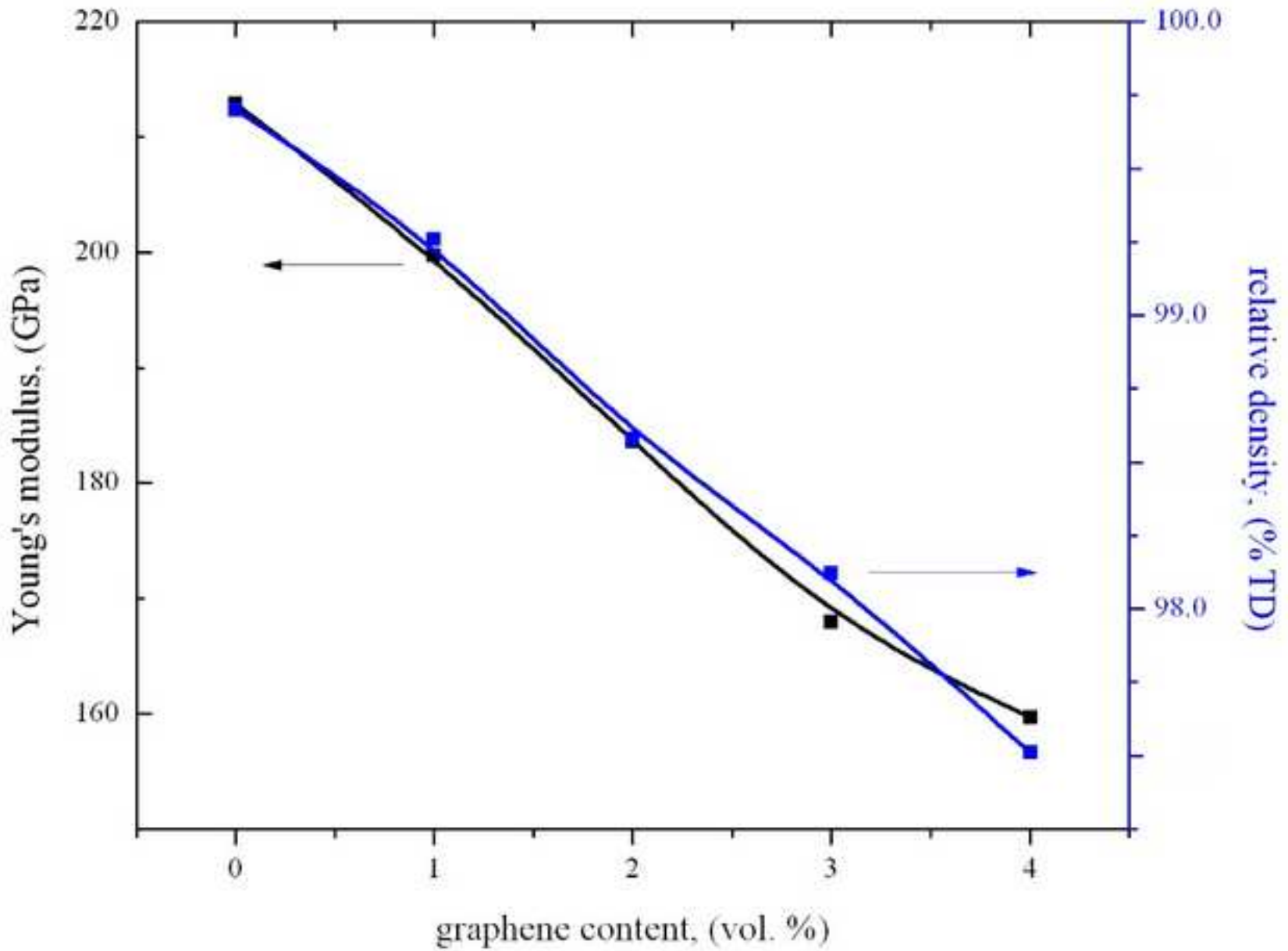

Figure
Click here to download high resolution image